Frictionally Modified Rotating Hydraulic Channel Exchange and Ocean Outflows*

GREGORY C. JOHNSON

Applied Physics Laboratory, University of Washington, Seattle, Washington

DANIEL R. OHLSEN

School of Oceanography, University of Washington, Seattle, Washington

(Manuscript received 5 October 1992, in final form 4 March 1993)

ABSTRACT

Laboratory experiments of two-layer exchange through channels of circular and half-circular cross section are described. Simple theoretical limits on exchange for the circular channels are obtained from models involving either friction or rotating hydraulic control alone. Ekman and Stewartson layers are appended to the rotating hydraulic control model in a simple theory for frictionally modified rotating control. In theory and experiment, rotation and friction together exert a stronger constraint on the exchange than they do separately. Secondary cross-channel circulations were found in the rotating experiments. These secondary circulations further reduce exchange by efficiently moving fluid that is spun down at the boundaries and interface into the interior. More accurate theoretical estimates of exchange must modify rotating hydraulics to include these frictional effects. Solid-boundary Ekman layers drove some of these secondary circulations; others were driven by robust interfacial Ekman layers. The interface in the rotating experiments had a cross-channel tilt since the exchange was geostrophic to first order. In the half-circular channel, the interface was sharpened on its deep side and spread on its shallow side by the strain field of the secondary circulations. In the presence of mixing, this strain field causes a wedge-shaped density field within the channel. A similar pattern has been observed in outflows through the Vema and Faroe Bank channels.

1. Introduction

Straits and channels connecting various ocean basins control the exchange of mass, heat, salt, nutrients, and other water properties between the basins. The most thoroughly studied is probably the Strait of Gibraltar, where an outflow of around $0.8 \times 10^6 \, \mathrm{m^3 \, s^{-1}}$ of dense, salty Mediterranean Water flows over the strait (Bryden and Kinder 1991) and forms a dense plume in the Gulf of Cadiz (Ochoa and Bray 1991). It has been argued that this outflow eventually contributes to high surface salinity in the Norwegian–Greenland Sea, allowing the formation of a dense component of the North Atlantic Deep Water (Reid 1979). A slightly larger amount of North Atlantic Central Water flows into the Mediterranean Sea at the surface, with the difference in the two transports going into the atmosphere through a net evaporation in the area (Bryden and Kinder 1991). (Throughout this paper, the dense layer near the bottom of a channel will be referred to

as the outflow and the light layer near the surface as the inflow.)

There are several possible constraints on outflows. The most widely investigated is inviscid hydraulic control, either for nonrotating two-layer exchange (Armi and Farmer 1989; Bryden and Kinder 1991) or for rotating reduced-gravity flow (Whitehead et al. 1974; Gill 1977; Borenäs and Lundberg 1986). Time dependence (Helfrich 1991), friction with and without rotation (Rydberg 1980; Pratt 1986), variations in channel shape and upstream condition (Borenäs and Lundberg 1986; Killworth 1992), and inviscid rotating two-layer exchange (Whitehead et al. 1974; Dalziel 1990) have all been explored and shown to have some influence on the rates of exchange in hydraulically controlled flow [see Pratt and Lundberg (1991) for a review].

In the South Atlantic, Lower Circumpolar Deep Water flows northward through the Vema Channel. An upper bound on the transport through this channel from inviscid rotating reduced-gravity theory significantly overpredicts the observed transport (Whitehead 1989). Density, velocity, and nephelometry measurements made within the channel indicate that a more complicated set of dynamics is needed to describe the outflow there (Johnson et al. 1976). There is an overall downward slope to the potential isotherms toward the

---

east, resulting in increasingly northward geostrophic velocities toward the bottom of the channel. (Throughout this paper the side of a channel where the pycnocline is deep will be referred to as the deep side and the side where the pycnocline is shallow as the shallow side.) At the deep side, the pycnocline is sharp, and below it is the coldest, most turbid water of the outflow. At the shallow side, the pycnocline is spread out, and geological evidence suggests rapid flow at the bottom. Near-bottom current meter data show a significant cross-channel flow toward the deep side, in the correct sense for flow within a planetary boundary layer.

Significant friction at the bottom and mixing at the pycnocline have been invoked to explain these observations (Johnson et al. 1976). It was proposed that bottom friction forces the coldest water toward the deep side of the channel, sharpening the pycnocline there. It was also suggested that strong flow at the shallow side induces mixing at the wall, spreading the pycnocline there. An alternative explanation for the wedge shape of the pycnocline involves inviscid rotating layered hydraulic control models (Hogg 1983). The sharpening at the deep side in these inviscid models results from the conservation of potential vorticity and Bernoulli potential in a narrowing channel. In contrast to the observations of Johnson et al. (1976), geostrophic velocity estimates indicate that the highest velocities in the outflow are found on the deep side, supporting the inviscid dynamics (Hogg 1983).

In the North Atlantic, there is a strong steady outflow of Arctic Intermediate and Norwegian Sea Deep Water into the Atlantic from the Norwegian Sea through the Faroe Bank Channel (Crease 1965; Borenäs and Lundberg 1988; Saunders 1990). Inviscid rotating hydraulic control theory applied to a parabolic channel with a motionless upper layer allows a reasonable prediction of the measured transport within a prescribed range of upstream interface heights (Borenäs and Lundberg 1988). A regional hydrographic survey reveals considerable mixing along the channel, resulting in downstream changes of water properties and heat flux of the outflow (Saunders 1990). There is also some inflow of North Atlantic Water above the outflow.

Vertical density and velocity profiles in the center of the channel sill indicate that the outflow and the inflow mix at the pycnocline that separates them, and that a thick planetary boundary layer is present at the bottom (Johnson and Sanford 1992). The isotherms are sharpened on the deep side of the channel and spread out on the shallow side [see Johnson and Sanford (1992), Fig. 6]. This shape is similar to that of the wedge-shaped pycnocline observed in the Vema Channel (Johnson et al. 1976). Johnson and Sanford (1992) suggest that cross-stream Ekman flow in the inflow on the deep side at the channel wall and at the bottom in the outflow meet at the pycnocline and then flow out into the interior. The resulting strain field would sharpen the pycnocline at its deep side. Obser-

vations indicate mixing and an interior flow within the pycnocline toward the shallow side. These dynamics would cause the pycnocline to spread toward the shallow side of the channel, as observed.

Benton and Boyer (1966) performed laboratory experiments to study rotating frictional one-layer flow through a circular channel. They found a secondary circulation, with cross-channel velocities at the top and bottom of the channel to the left looking downstream, and a nearly uniform interior return flow. They discussed the dynamics of these modified Ekman layers at the walls. For frictional rotating one-layer flow through a rectangular channel, Hart (1971) observed a similar set of double-vortex secondary circulations. He also analyzed a longitudinal roll instability found at intermediate rotation rates. Whitehead et al. (1974) presented laboratory results for two-layer exchange through a rectangular gap in a wall. Transport measurements in this limit are in good agreement with those predicted by an inviscid rotating hydraulic control theory because their experiments minimized friction.

In our experiments, both rotation and friction were important in two-layer exchange through channels of circular and half-circular cross section. Results from control runs where friction or rotation were independently dominant show that exchange was smallest with both effects present. The Ekman layers in the channels drove strong secondary circulations which efficiently limited the exchange. Dye introduced in the bottom Ekman layer at one end of the channel completed a full turn through a helical path as it passed through the channel. Ekman layers were observed at the solid boundaries. In addition, evidence for robust Ekman layers at the layer interfaces was found. In each layer of the circular channel, a double vortex pair of secondary circulations similar to that observed by Benton and Boyer (1966) and Hart (1971) were driven by these two boundary layers. The separation point for flow to return to the interior of each layer was along the interface, suggesting that the solid-boundary Ekman layer was the stronger of the two. In the half-cylinder, the secondary circulations in the outflow were similar to those found in the cylinder. However, the secondary circulation in the inflow differed from that in the cylinder, since the interfacial and solid-boundary Ekman layers drove a single secondary circulation.

2. Experimental design and technique

The experimental apparatus was constructed mostly of Plexiglas. It consisted of a rectangular tank of approximate dimensions 120 cm long by 30 cm wide by 40 cm high, partitioned into two reservoirs by a vertical dam (Fig. 1). The tank was centered on a rotating table. The two reservoirs were connected by a channel piercing the dam. The channel was either of circular cross section located at middepth (Fig. 1a, the tube), or of open half-circular cross section located near the
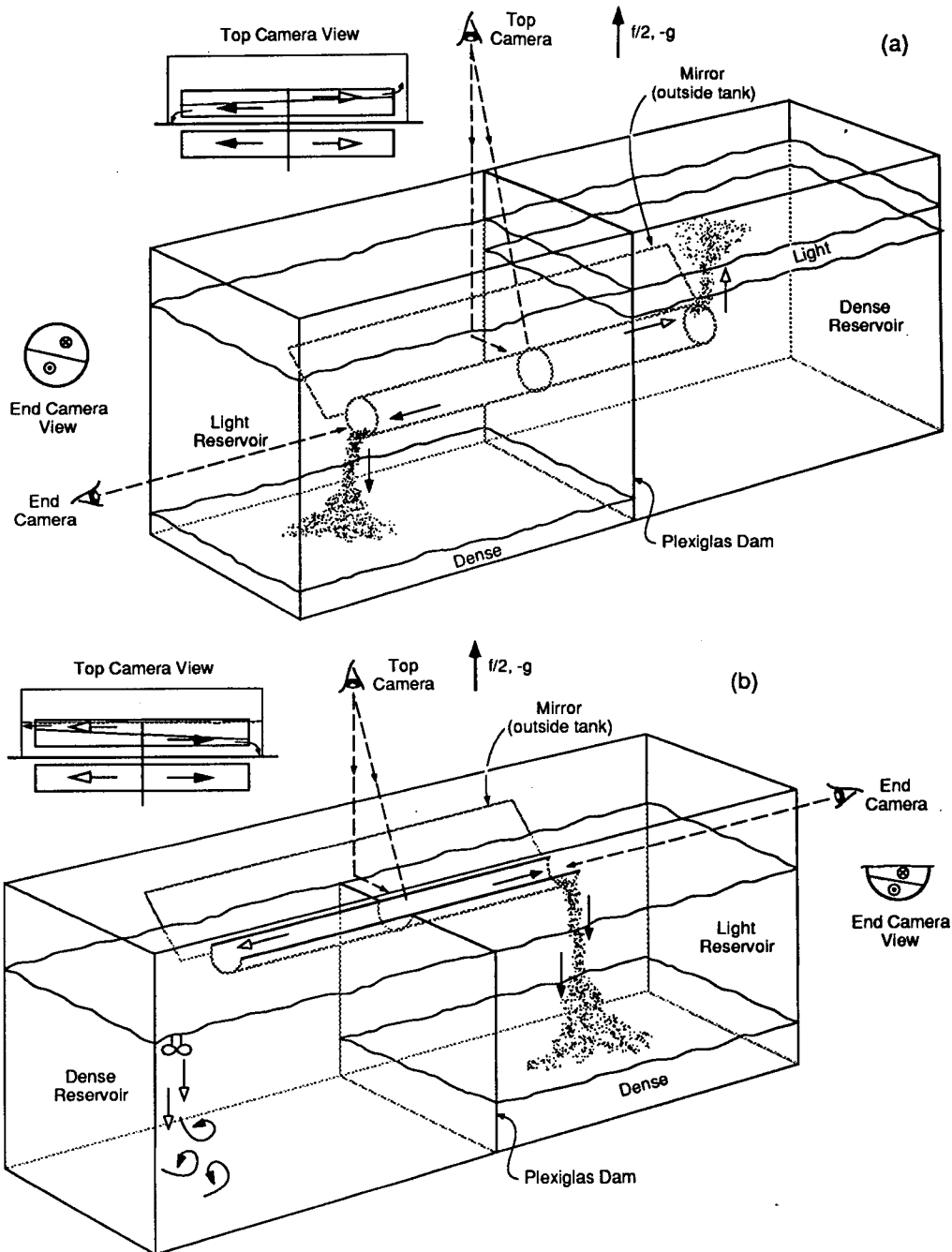
FIG. 1. Experiment schematics. Fluids of different densities are separated by the Plexiglas dam at the start of the experiment. The channel is opened and two-layer exchange through the channel is photographed from the top, side (with mirror), and end. (a) Tube experiments. The dense outflow (solid arrows) flows over the tube bottom into the light water reservoir. The light inflow (open arrows) flows through the upper part of the tube and enters the dense water reservoir. (b) Trough experiments. The dense outflow spills into the light reservoir. A pump mixes the light inflow into the dense reservoir.

free surface (Fig. 1b, the trough). These configurations allowed us to study two-layer reduced gravity rotating exchange flow with either a solid or a free surface.

The tube had an inside diameter of 4.4 cm and a length of 62 cm. It was centered in the dam lengthwise, parallel to the tank walls, and one end was stopped before the reservoirs were filled. Each side was filled to a depth of 25.4 cm with room temperature water of a different salinity. The table was rotated at a constant rate and the fluids within the tank were allowed to

come into roughly solid-body rotation. When the cork was removed, the outflow moved from the dense water reservoir toward the light water reservoir, inside the lower portion of the tube. The inflow moved in the opposite direction inside the upper portion of the tube. The outflow exited the tube and spilled down toward the bottom of the light reservoir, filling it slowly from the bottom up with dense water. Similarly, the inflow exited the tube but rose to the top of the dense reservoir. The runs usually lasted for about a half hour, until the fluids entering each reservoir filled them to such a level that these fluids were almost reentering the tube to flow back toward their original reservoirs. The tube was again stopped at one end at this point. Two control runs were performed, one with rotation but with a tube 0.9 cm long so that friction was much reduced, and the other with a long tube but no rotation. Runs with both friction and rotation were carried out at three different density differences.

For the other configuration, a Plexiglas tube 62 cm long with an inside diameter of 7 cm was sawed in half along its axis to create a half-circular trough (Fig. 1b). The trough was centered in the tank, parallel to the walls and bottom. Its edges were flush with the top of the dam, just above 25.4 cm off the bottom of the tank. Cutting the tube in half resulted in a trough slightly deformed from a half-cylinder. The trough width at the free surface was 6.7 cm. The deepest point in the trough was 3.5 cm from the free surface, resulting in a total cross-sectional area similar to that of the tube. This configuration was intended to represent straits such as the Faroe Bank and Vema channels. The light inflow was mixed into the dense reservoir by a pump to keep the inflow from rapidly filling that reservoir to the depth of the trough bottom, shutting down the exchange. This mixing caused a gradual change in the density difference but allowed the runs to continue for over half an hour, much longer than without the pump. When the dense fluid filling the bottom of the light reservoir nearly reached the trough bottom, the trough was blocked and the experiment was stopped. To allow a more turbulent exchange, one experiment was conducted with a right triangular trough 100 cm long, 8 cm deep, and 16 cm wide.

In the tube configuration, the salinity, S, and temperature, T, were measured in each reservoir before each run. Vertical profiles of these quantities were measured throughout the run so that it could be stopped before fluids that had moved once through the tube began reentering it. After each run, the reservoirs were stirred and S and T measured again. Although the water temperature often increased as much as 1°C during a run, salt was conserved. The exchange through the tube consisted solely of fluids with their initial salinity, hence the average initial and final (denoted by subscripts i and f) salinity in each reservoir can be used to estimate the average volume transport over the elapsed time, t, of the run. Using the conservation of volume and salt,

$$Q = \frac{(S_{lf} - S_{li})V}{(S_{di} - S_{li})t}$$

allows an estimate of the volume transport (or exchange) through the tube, Q, in either direction. Here V is the volume of one of the reservoirs (both of V = 4.6×10^4 cm^3). Subscripts l and d refer to the light and dense reservoirs, respectively. These estimates are biased slightly low owing to the neglect of mixing between the layers within the channel.

Top, side, and end views of the flows were photographed (Fig. 1). The flow was visualized in two different ways. Dyed water was injected in various locations in the inflow and outflow to mark water parcels and create dye streaks. These streaks reveal the helical patterns of water parcels flowing through the channels driven by Ekman layers within the channels. In some runs, disodium fluorescein was used to reveal mixing between the fluids within the channel (Breidenthal 1981; Koochesfahani and Dimotakis 1986). The dye is pH sensitive, only fluorescing above about pH 4. The dye was added to one reservoir at a concentration of about 2×10^{-6} M along with hydrochloric acid to bring the fluid to pH 3.7. Sodium hydroxide was added to the other reservoir to bring it to pH 11.6. Thus one part of the basic fluid would make twenty parts of the dyed acid fluid fluoresce. This volume ratio of 20 suppressed any reversal of the reaction and kept mixed fluid fluorescing. A cross section of the channel was illuminated by a thin (1 cm) sheet of white light. An end view of the region of fluorescence shows mixing at the interface and reveals the presence of interfacial Ekman layers.

3. Scaling and theory

We develop a scaling for the laboratory experiments based on the size of various parameters inferred from observations made in the Faroe Bank Channel outflow. A simple two-dimensional theory for nonrotating frictional two-layer exchange through a tube is presented. An existing theory for inviscid rotating two-layer exchange is adapted to the tube experiments. This inviscid rotating theory is then further modified to include reductions in the alongchannel velocity field by frictional rotating boundary layers. The limitations of these rather simple theoretical frameworks are discussed.

a. Scaling

The experimental parameters used in the laboratory were determined using the following information gained from oceanographic observations. In the Faroe Bank Channel outflow, the depth of the planetary boundary layer is a significant fraction of the outflow depth, and the Rossby number approaches unity

(Johnson and Sanford 1992). Since the outflow is probably subject to hydraulic control (Borenäs and Lundberg 1988), the Froude number is near unity. The internal Rossby radius of deformation is about the channel width. Finally, the spindown time is about the time it takes for a water parcel in the outflow to move through the channel (Johnson and Sanford 1992).

The flow in the laboratory was observed to be laminar so molecular viscosity, $\nu = 1.0 \times 10^{-2}$ cm^2 s^{-1}, is used in the scaling. The tube diameter is $L = 4.4$ cm, resulting in a layer depth of $H = 2.2$ cm. A Coriolis parameter of $f = 0.67$ s^{-1} is used, resulting in a total Ekman depth that is one-quarter of the layer depth, $\pi(2\nu/f)^{1/2} = H/4$. Taking the density difference between the inflow and outflow to be $\Delta\rho = 5.7 \times 10^{-3}$ g cm^{-3}, with gravitational acceleration $g = 980$ cm s^{-2}, and average density of the two layers $\rho = 1.0$ g cm^{-3}, gives a reduced gravity $g' = g\Delta\rho/\rho = 5.6$ cm s^{-2}. Assuming that the exchange is subject to hydraulic control implies a composite Froude number, $(\Delta U)^2/2g'H$, of near unity. Gill (1977) showed that a more involved formulation holds formally for rotating hydraulic control. However, the simple formulation is used here in scaling the velocity difference between the inflow and outflow, so $\Delta U = 5.0$ cm s^{-1}. Hence the Rossby number, $\Delta U/2fL = 0.8$, is also near unity.

The internal Rossby radius of deformation, $x_0 = (g'H)^{1/2}/f = 5.2$ cm, is about the tube diameter. The spindown time is $H(2/f\nu)^{1/2} = 38$ s. If the velocity in each layer, $\Delta U/2$, is close to 2.5 cm s^{-1}, then the tube length should be about 95 cm for the spindown time to be close to the time it takes a water parcel to travel through the tube. (In practice, velocities were less than predicted, probably owing to alongstream variations in the velocity and density fields. Hence a tube length of 62 cm was used.) A crude prediction of the exchange rate Q is half the velocity difference times half the cross-sectional area of the tube, or 19.0 cm^3 s^{-1}.

Finally, the height of the free surface relative to that at the center of rotation is $\eta = (fr)^2/8g$, where r is the radial distance from the center. With the scaling parameters used above, the deformation height at the channel ends, $r = 31$ cm, would be only $\eta = 0.06$ cm. Since this height difference is about 1% of the tube diameter or trough depth, the effect is negligible.

b. Nonrotating frictional theory

Nonrotating, steady, frictional flow through a pipe subject to a uniform pressure gradient is known as Poiseuille flow (Batchelor 1967). An equation for the velocity is found by assuming that the flow is laminar and unidirectional, and that the stress, which brings the velocity in the pipe to zero at the boundaries, balances the pressure gradient. The resulting Poisson equation is easily solved in cylindrical coordinates. Here the differing reservoir densities result in a pressure gradient along the tube that is zero along the horizontal

diameter at the center of the tube. This gradient increases linearly with vertical distance from this diameter. It reaches maximum equal and opposite values at the top and bottom of the tube center. Significant variations along the tube length, λ, are observed, but here we ignore them to find an approximate governing equation for flow along the tube,

$$\frac{1}{r}\frac{\partial}{\partial r}\left(r\frac{\partial u}{\partial r}\right) + \frac{1}{r^2}\left(\frac{\partial^2 u}{\partial\theta^2}\right) = \left(\frac{g'r}{\nu\lambda}\right)\sin\theta.$$

Here u is the alongchannel velocity, r the radial distance from the tube center, and θ the angle from the horizontal. The right side of the equation is proportional to the depth-dependent alongtube pressure gradient. Subject to the boundary conditions that the flow vanish at the edge of the tube and be well behaved in the interior, the solution for the alongchannel velocity is

$$u = \left(\frac{g'}{\lambda\nu}\right)\left[\frac{r^3\sin^3\theta}{6} - \frac{a^2 r\sin\theta}{8} + \frac{r^3\sin3\theta}{24}\right],$$

where a is the tube radius.

The maximum speed in either layer for this solution is $u_{max} = (g'a^3)/(12\sqrt{3}\nu\lambda)$. For $\lambda = 62$ cm with the scaling values given above, the maximum velocity is 4.6 cm s^{-1} (Fig. 2). The velocity can be integrated over the cross-sectional area of either layer to find the volume transport, $Q = (g'a^5)/(30\lambda\nu)$. The predicted transport is 15.5 cm^3 s^{-1}. Thus, the maximum frictional velocity is twice the average velocity from the
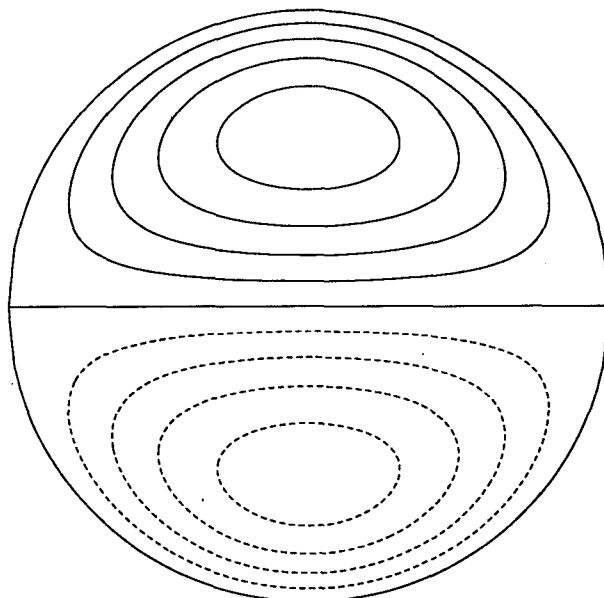

FIG. 2. End view of isotachs of steady two-dimensional frictional two-layer flow in a tube. Tube radius $a = 2.2$ cm, reduced gravity $g' = 5.6$ cm s^{-2}, tube length $\lambda = 62$ cm, and viscosity $\nu = 0.01$ cm^2 s^{-1}. The velocity, contoured at 1 cm s^{-1} intervals, is of opposite sign above and below the horizontal interface.

inviscid rotating hydraulic scaling $\Delta U/2 = 2.5$ cm s^{-1}, but the transport, hence mean velocity, is similar. The frictional transport and velocity are both proportional to the pressure difference (linearly related to the reduced gravity) over the tube length. The tube radius comes in at the third power in the velocity and the fifth power in the transport. Hence, a narrow tube restricts exchange more than a long one.

c. Inviscid rotating hydraulic control theory

A theory for inviscid rotating hydraulic two-layer exchange was developed by Whitehead et al. (1974). The reservoir depth in our experiment is ten times the tube diameter, effectively infinite as in their theory. The tubular channel with diameter 4.4 cm in the experiment is approximated by a square channel 3.9 cm on a side in the theory, conserving cross-sectional areas. Following Whitehead et al. (1974), $L = 1.95$ cm is the half-width of the square channel, not the tube diameter, and $H = 3.9$ cm is the channel depth, not the layer depth. The net transport of the outflow with this theory is

$$Q = \frac{1}{2}(g'H)^{1/2}HL\left(1 - \frac{1}{3}\frac{L^2}{x_0^2}\right),$$

where the Rossby radius, $x_0 = (g'H)^{1/2}/2f = 5.2$ cm, is greater than L (the case here). The predicted velocity difference between the inflow and outflow is 4.7 cm s^{-1} and the predicted volume exchange, 16.9 cm^3 s^{-1}.

d. Frictionally modified rotating hydraulic control theory

A complete theory for frictionally modified rotating two-layer hydraulic control in a tube is beyond the scope of this investigation. The approach here is two-dimensional and very simple: We modify the two-layer inviscid rotating hydraulic control theory outlined above to include some of the effects of friction. Ekman layers are appended to the top and bottom of each layer in the square channel, and Stewartson layers to their sides (Pedlosky 1979). Each interfacial Ekman layer is assumed identical to the top or bottom Ekman layer (neglecting the geostrophic cross-channel slope at the interface). Only the effects of the alongchannel component of velocity on the transport are included. The cross-channel secondary circulations driven by these Ekman layers inject water with retarded velocities out from the boundaries into the interior. Thus, the neglected cross-channel circulations likely play a significant role in further reducing the exchange.

The net transport of the outflow for the inviscid rotating theory, modified to account for reductions in the downstream velocity field owing to the presence of rotating boundary layers, is

$$Q = \frac{1}{2}(g'H)^{1/2}HL\left(1 - \frac{1}{3}\frac{L^2}{x_0^2}\right) - (g'H)^{1/2}Lz_0$$
$$- (g'H)^{1/2}\frac{H}{4}\sigma\left(1 - \frac{L}{x_0}\right)$$
$$\times\left[1 + \frac{L-\delta}{x_0} - \left(1 - \frac{\delta}{x_0}\right)\exp(-L/\delta)\right]$$
$$- (g'H)^{1/2}\frac{H}{4}\delta\left(1 + \frac{L}{x_0}\right)$$
$$\times\left[1 - \frac{L-\delta}{x_0} - \left(1 + \frac{\delta}{x_0}\right)\exp(-L/\delta)\right].$$

The first term on the right side of the equation is from the inviscid theory discussed above. The second term doubles the effect of the alongstream component of the solid-boundary Ekman layer on the transport to account crudely for both it and the interfacial Ekman layer. Here $z_0 = (2\nu/f)^{1/2} = 0.17$ cm is the vertical decay scale of the Ekman layer. The last two terms account for the presence of Stewartson layers, in the outflow at the deep and shallow sides, respectively. The horizontal decay scale for the Stewartson layer is $\delta = (2\nu H^2/f)^{1/4} = 0.58$ cm. The Stewartson layers are fairly thick and slightly modify the interior velocity field out to the center of the channel. Including the reduction of the interior velocity by the Stewartson layer as a boundary condition for the Ekman layer calculations would further reduce the transport by a small amount. The theory is already quite approximate, so this correction is not included.

Using the parameters introduced in the scaling above, the frictionally modified rotating hydraulic control theory predicts a transport of 10.8 cm^3 s^{-1}. Since the transport predictions cited earlier fall within the range 17 ± 2 cm^3 s^{-1}, this value is about two-thirds that predicted by the other theories. The scaling estimate and that from the model for inviscid rotating hydraulic two-layer exchange should agree because setting the Froude number to unity in the scaling assures hydraulic control in each case. The tube length is chosen such that the nonrotating frictional transport estimate agrees roughly with both of the rotating inviscid estimates. However, the approximate frictionally modified rotating hydraulic control theory predicts significantly less transport than the other theories. In contrast to the nonrotating frictional theory, the channel length does not affect this exchange calculation.

4. Experimental results

The experimental results are presented in two subsections. In the first we detail the measurement of exchange through the tube for various values of Coriolis parameter, tube length, and reduced gravity. The exchange is estimated using salt and volume conservation,

as detailed above. The results are discussed with regard to transport predictions from the theories. In the second subsection, we discuss the observed secondary circulations. Evidence of robust interfacial and solid-boundary Ekman layers, each driving a secondary circulation, is presented. Secondary circulations observed in the tube are contrasted with those in the trough. Finally, results from a trough experiment at large Reynolds numbers are contrasted with results from the laminar experiments.

a. Exchange through the tube

In run 1 the reduced gravity was 5.4 cm s^{-2} and the Coriolis parameter 0.67 s^{-1}, but the tube length was only 0.9 cm. This run is best compared with results from the two-layer inviscid rotating hydraulic control theory (Whitehead et al. 1974). The measured transport for this run was about four-fifths of that predicted by the theory (Table 1). This difference is slightly larger than the experimental error, which is no more than 10%. However, even in a tube 0.9 cm long there will be some retardation of the exchange owing to friction at the boundaries and at the interface. Also, the circular tube used in the laboratory is approximated in the theory by a square of identical cross-sectional area. Considering these differences, the experimental results and theory are in good agreement.

In run 2 the reduced gravity was 5.6 cm s^{-2} and the tube length 62 cm, but there was no rotation. This run is best compared with the nonrotating frictional theory above. The measured transport is less than one-half of that predicted (Table 1). There are at least three possible reasons for this discrepancy, all related: First, for the parameters of run 2, flow must move a distance of at least the tube length to accelerate from rest to Poiseuille flow (Prandtl and Tietjens 1934). Thus, two-dimensional theory that assumes fully developed frictional flow is not completely valid. Second, in all the runs with a long channel, there is a significant alongchannel slope to the interface that indicates an approximate balance among acceleration, friction, and

changing interface height. This alongchannel variation in interface height is such that the outflow is about two-thirds of a diameter thick at its entry and one-third of a diameter thick at its exit. Hence, the cross-sectional area of the tube at the exit for each layer is about four-sevenths of that used for the two-dimensional theory. Third, since the flow is not fully frictional the layers may be subject to hydraulic control at their exits, where the velocity is large and the layer depth small, giving a large Froude number. None of these factors are included in the simple two-dimensional frictional theory.
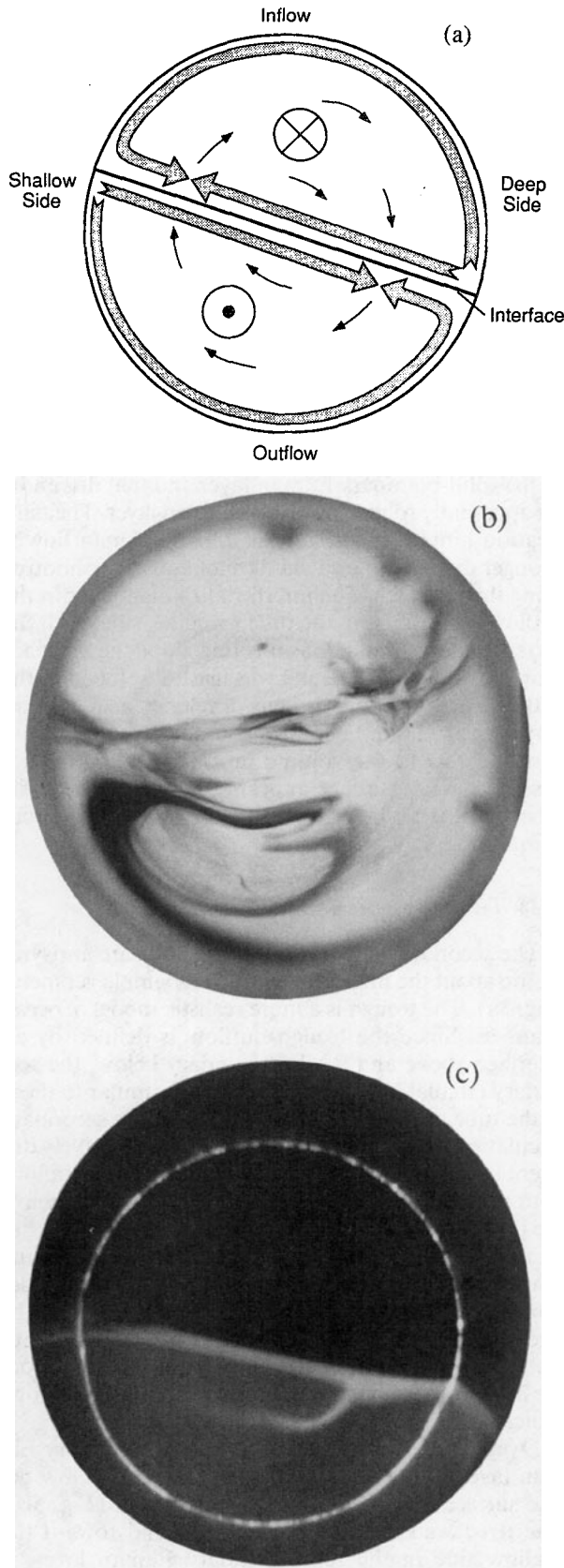
Runs 3–5, with both rotation and friction, had reduced gravity values of 3.5, 5.6, and 7.1 cm s^{-2}. The measured transports vary roughly linearly with the reduced gravity (Table 1). The observed values are again only about one-half of those predicted by the approximate frictionally modified rotating hydraulic control theory. Again, this discrepancy is probably owing to three related factors, similar to those outlined above for the dominantly frictional case. The observed transport with friction and rotation and the appropriate reduced gravity is even less than that for the runs where either friction or rotation predominate (Table 1). This further reduction in exchange probably results from the neglected cross-channel secondary circulation described below, which efficiently moves spundown fluid at the solid boundaries and interface into the interior. Thus rotation and friction combine to provide the strongest constraint on two-layer exchange.

b. Secondary circulations

The experimental results presented above are consistent with Whitehead's (1989) Table 1 indicating that the upper bound on transports through various sills and channels in the ocean from inviscid rotating hydraulic control theory overestimates the observed flows through these straits considerably. We suggest the rotating frictional cross-channel secondary circulations force spundown fluid into the interior, further limiting the exchange by a mechanism not included in our sim-

TABLE 1. Experimentally determined and predicted exchange rates for a tube of 4.4 cm inside diameter. The first four columns identify the run, reduced gravity, tube length, and Coriolis parameter. The fifth column, in **boldface**, reports exchange rates (in cm^3 s^{-1}) measured for flow through the tube. The last three columns contain, respectively, transports predicted from inviscid rotating hydraulic control theory, nonrotating frictional theory, and fractionally modified rotating hydraulic control theory. The predicted transport appropriate to the observed value for each run is in **boldface**. Theories that are not applicable to the control runs are denoted by n.a. The predictions of three theories are calculated for runs 3–5 for comparison.

	Run numbers and conditions			Observed and predicted transports			
Run	g' (cm s^{-2})	Length (cm)	f (s^{-1})	Observed (cm^3 s^{-1})	Rotation (cm^3 s^{-1})	Friction (cm^3 s^{-1})	Both (cm^3 s^{-1})
1	5.36	0.9	0.67	**13.3**	**16.5**	n.a.	n.a.
2	5.59	62.0	0.0	**7.0**	n.a.	**15.5**	n.a.
3	3.48	62.0	0.67	**3.6**	13.0	9.6	**8.4**
4	5.60	62.0	0.67	**5.5**	16.9	15.5	**10.8**
5	7.11	62.0	0.67	**6.2**	19.3	19.7	**12.2**

FIG. 3. End views of rotating exchange flow in a tube (Fig. 1a). (a) Schematic. Alongchannel geostrophic flow results in a tilted interface with a deep (right) and shallow (left) side. The outflow (lower layer) moves out of the page. Ekman flow at the periphery of each layer (shaded arrows) is to the left looking downstream. Interior return flow (small arrows) is in the opposite direction. (b) Dye streak in the lower outflow secondary circulation [viewed from the end opposite (a) and (c)]. The streak describes one turn of a clockwise helical path starting from the shallow side of the outflow entry (middle right). The streak is reflected on the tube bottom when in the interior. (c) Fluorescein in the outflow. A 1-cm thick cross section is illuminated 19 cm from the outflow exit. Fluid in the outflow that has mixed with that in the inflow is fluorescent. The fluorescent tail that extends down from the interface near the deep side and curls toward the shallow side in the interior marks the boundary between the secondary circulations.

ple frictional modification of the rotating hydraulic theory. These secondary circulations are described below. The alongchannel flow in the experiments was observed to be in geostrophic balance to lowest order. Solid-boundary and interfacial Ekman layers drove cross-channel secondary circulations. The secondary circulations were observed both in the tube and the trough. The trough, with its upper free surface, is meant to approximate ocean straits and channels. In the trough, especially in a high Reynolds number run, the cross-channel flows maintained a wedge-shaped interface similar to those commonly observed in the pycnocline in ocean straits.

1) THE TUBE

Within the tube, two strong secondary circulations were observed in each layer (Fig. 3). Interfacial and solid-boundary Ekman layers drive flow to the left looking downstream at the periphery of each layer. Interior return flow to the right looking downstream closes the secondary circulations. In each layer the solid-boundary Ekman layer overshoots about one-quarter diameter along the interface until stopped by the interfacial Ekman layer moving in the opposite direction. This overshoot may occur because the solid-boundary Ekman layer is stronger than the interfacial Ekman layer, owing to mixing at the interface, stratification at the interface, or stronger friction at the solid boundary. Mixed fluid moves away from the interface at the juncture of the two Ekman layers and then to the right looking downstream in the interior. These secondary circulations form two vortices of opposite signs in each layer.

To visualize the flow, dyed water was injected into the solid boundary Ekman layer of the outflow near its entry, at the shallow side of the tube, with the resulting streaks giving insight into the water's motion (Fig. 4). Near the injection site the dye streak runs slowly downstream and toward the deep side in the solid-boundary Ekman layer at an angle about $-30°$
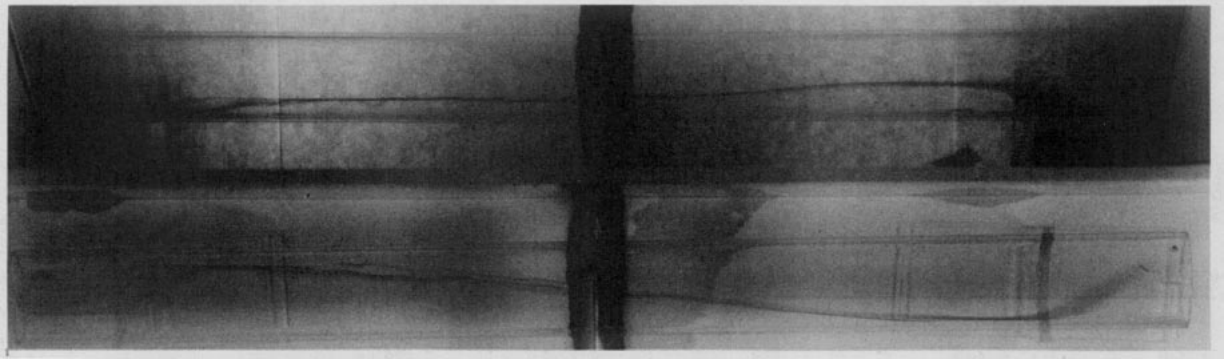
FIG. 4. Top and side view of a dye streak in the tube outflow. The camera was above the tank, with a mirror revealing the side view at the top of the photograph (Fig. 1a). The outflow moves from right to left. Dye was injected in the solid-boundary Ekman layer at the shallow side in the outflow near its entry (right side). The dye streak describes about one turn of a roughly helical path as it moves along the tube.

from downstream. Dye streaks likely do not follow exactly the motion of a water parcel within the boundary layer, but this angle is consistent with that expected for flow near the bottom of an Ekman layer. Once the dye climbs the tube wall to the interface, it travels about two tube diameters farther down the tube along the wall and then moves rapidly downstream and slowly toward the shallow side in the interior of the outflow at an angle of about 7° from downstream in the interior. These angles of deviation from downstream indicate a cross-stream interior return flow about four times slower (hence thicker) than that in the bottom Ekman layer. Near the outflow exit the dye streak reaches the shallow side of the tube and then moves back toward the deep side in the solid-boundary Ekman layer just before exiting the tube, having described one turn through a roughly helical path within the tube. The fluid undergoes about one spindown as it transits the tube.

The dyed water has a tendency to move away from the interface as it moves down and toward the shallow side in the interior return flow (Fig. 3b). This motion results from the presence of a smaller interfacial Ekman layer that drives a flow toward the deep side along the interface, with an interior return flow toward the shallow side. The secondary circulation driven by the interfacial Ekman layer was difficult to visualize clearly with dye injections, but it did yield to the visualization technique below.

Fluorescein dye indicates mixing between the inflow and outflow as described above. The dense reservoir was made acid and dyed; the light reservoir was made basic. The light sheet illuminated a vertical cross section of the tube that was viewed from the tube end (Fig. 3c). The fluorescing, mixed fluid at the interface is thin, suggesting that there is little turbulent mixing there. The remarkable tail of mixed fluid in the outflow that extends away from the interface near the deep side and curls toward the shallow side in the interior marks the separation between the secondary circulation driven

by the solid-boundary Ekman layer and that driven by the apparently robust interfacial Ekman layer. The tail's location hints that the solid-boundary Ekman flow is stronger than the interfacial Ekman flow, overshooting along the interface. The interfacial Ekman layer in the outflow is confined to the tube's shallow side, with the two secondary circulations meeting along the interface near the deep side. The tail was least developed at the outflow entry and very strongly developed near the exit. Any similar tail in the inflow would be about 20 times fainter owing to the volume ratio used, and was not observed. The interface appears to level out near the tube walls, perhaps owing to the cross-channel circulations (Fig. 3a).

2) THE TROUGH: LAMINAR CASE

The secondary circulations in the tube are antisymmetric about the interface owing to its simple geometry (Fig. 3a). The trough is a more realistic model of ocean channels. Since the trough outflow is defined by an interface above and a solid boundary below, the secondary circulations observed there are similar to those in the tube outflow (Fig. 5a). However, the secondary circulation within the trough inflow is qualitatively different from that in the tube inflow. In the trough inflow, both the solid boundaries and the interface are below the flow. Hence the solid-boundary and interfacial Ekman layers drive a single flow to the left (looking downstream), resulting in a single secondary circulation. While there should be little Ekman flow at the free surface, some flow is seen there in the experiments. This flow varies in direction along the channel, as does the height of the interior return flow. The dashed arrows indicate this variation (Fig. 5a).

Dyed water was injected in the solid-boundary Ekman layer of the inflow near its entry, just below the free surface at the deep side of the trough (Fig. 5b). The dyed water moves downstream and toward the shallow side in the solid-boundary Ekman layer. It
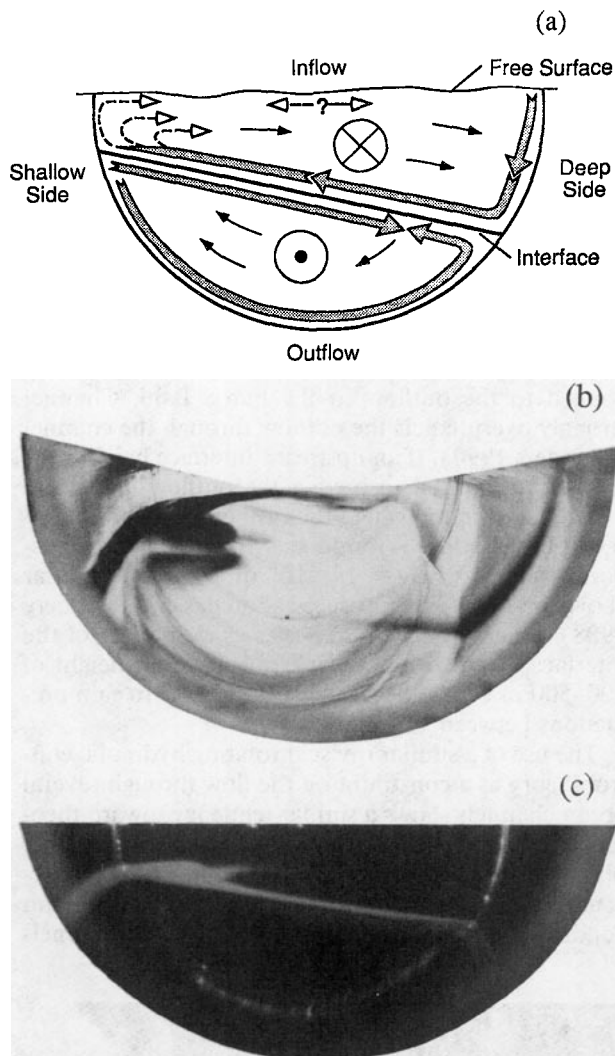
(a)

(b)

(c)

FIG. 5. End views of rotating exchange flow in a trough (Fig. 1b). (a) Schematic. The geostrophic alongchannel flow supports a tilted interface. The outflow (lower layer) moves out of the page. Its secondary circulations are similar to those found in the bottom layer of the tube (Fig. 3a). In the inflow, Ekman flows (shaded arrows) are all toward the shallow (left) side, driving a single secondary circulation. Alongchannel variations in the interior return flow are represented by the dashed arrows. (b) Dye streak in the trough inflow. Dye was injected into the solid-boundary Ekman layer near the inflow entry at its deep side just below the free surface (upper right). The dye streak describes roughly one turn of a clockwise helical path. At the interface the streak is dispersed by the alongchannel vertical shear there. (c) Fluorescein in the trough inflow. The light sheet was 27 cm from the inflow entry. Inflow water that has mixed with outflow water is fluorescent. Mixed fluid is banked up at the shallow side above the interface. A tail of mixed fluid extends toward the deep side in the inflow interior.

crosses the interface in the interfacial Ekman layer, but is dispersed by the strong vertical shear there. The dye is again visible at the trough wall on the shallow side. It hugs the wall there for a greater distance than in the tube, and some of it slowly flows back toward the inflow

entry along this wall, reversing downstream direction as it joins the outflow. The streak eventually enters the interior of the inflow and flows slowly back toward the deep side as it moves downstream.

For a visualization of the mixed fluid in the inflow, near the interface, the light reservoir was made acid and dyed with fluorescein and the dense reservoir was made basic, as outlined above. A vertical light sheet illuminated a cross section of the trough that was viewed from the trough end (Fig. 5c). As the injected dye suggests, the mixed fluid at the interface tends to collect on the shallow side of the inflow, banking against the wall there. This mixed fluid entered the interior at various heights ranging from near the interface level around the inflow entry to near the free surface within 10–15 cm of the inflow exit (Fig. 5a). The variation may be caused by development of the secondary circulation as the inflow passes through the trough, end effects, or flow from the pump.

3) THE TROUGH: TURBULENT CASE

In the Faroe Bank Channel, the pycnocline is sufficiently weak and the vertical shear sufficiently strong for the development of turbulent shear instabilities (Johnson and Sanford 1992). This is not the case for the experiments discussed above. Turbulent mixing begins at interfacial Reynolds number of order 2000 (Breidenthal 1981). It is difficult to scale the flow in the laboratory such that the interfacial Reynolds number based on interface thickness, velocity difference, and molecular viscosity (order 10 in these experiments) is sufficiently high to allow strong mixing, while maintaining an Ekman layer thickness that is a significant fraction of layer depth.

One set of experiments was carried out in which the Reynolds number was increased to around 2000 at the expense of the Ekman number and strength of friction. The configuration was that of the trough (Fig. 1b), except that a right triangular channel about 100 cm long, 8 cm deep, and 16 cm wide was substituted for the semicircular one, giving a cross-sectional area about 3.5 times that of the original trough. In addition, the level of the dam and the fluid in the tank was raised such that there were about 62 L on each side. Fluorescein was used as before for visualizing mixing at the interface, except at a volume ratio of 10, to allow some (still weak) visualization of mixing in the outflow. Isopropanol was used in the light reservoir and salt in the dense reservoir to obtain $g' = 49$ cm s^{-2}, about nine times that used before. The proportions of these additives were calculated to give equal indices of refraction in the two reservoirs. The rotation rate was increased so $f = 1.0$ s^{-1}. In this case, the Ekman layer depth is only about one-tenth of the layer depth. The Rossby number is still order one, while the velocity difference reaches 20 cm s^{-1}. The internal Rossby radius of deformation is still about the channel width,

but the spindown time is now about ten times the time it takes a water parcel to flow through the tube. Hence the flow is more likely to be subject to hydraulic control. The transport predicted from this scaling is about 320 $cm^3 s^{-1}$. The experiment ran for about 3 minutes.

The flow in this experiment was turbulent, with eddies visible on the interface. The flow appeared to be subject to hydraulic control, with no visible along-channel slope to the interface and standing alongchannel waves on the interface that broke on occasion. The mixed fluid in the inflow was swept from the deep to the shallow side by the secondary circulation (Fig. 6). Some evidence of the strong eddy motion is visible. Only a very faint tail of mixed fluid extends from the deep to the shallow side in the outflow just below the interface. This tail is sharpened at the deep side, and fades as it spreads toward the shallow side. The wedge-shaped interface was robust, enduring throughout the experiment. It was presumably generated by cross-channel secondary circulations sharpening the deep side of the interface and spreading the shallow side of the interface with the mixing. This wedge shape is strongly reminiscent of the pycnocline in the Faroe Bank Channel [compare Fig. 6 with Johnson and Sanford's (1992) Fig. 6] and the Vema Channel (Johnson et al. 1976). This shape also appears in layered inviscid rotating hydraulic control models (Hogg 1983). Thus, pending further field studies the dynamical origin of this wedge shape in the ocean is still open to debate.

5. Discussion

The experimental results presented demonstrate that in a long, thin channel, like many of those connecting various ocean basins, both friction and rotation can play an important role in controlling exchange between the basins. The measured transport in the nonrotating frictional run is about one-half of that for the "inviscid" rotating run (Table 1). The run with both friction and rotation shows an exchange reduced to two-fifths of the "inviscid" rotating run. In both theory and experiment, friction and rotation together exert a stronger constraint on exchange than either does separately. These results agree with investigations of the flow in the Bornholm Channel (Lundberg 1983; Gidhagen and Håkansson 1992).

It has been argued that the purely rotating theory applied to the outflow in the Faroe Bank Channel strongly overpredicts the outflow through the channel (Saunders 1990). If an upstream interface height near the surface is used to predict the outflow (there are locations upstream where the isotherm chosen to represent the interface is found near the surface), a transport of 8.8 Sv (1 Sv $\equiv$ 1 $\times$ 10^6 $m^3 s^{-1}$) is found, far above the 1.4–1.9 Sv measured (Borenäs and Lundberg 1988). Since the transport scales as the square of the interface height in the theory, an upstream height of 400–500 m below the surface can be used to gain predictions between 1.5–2.5 Sv.

The use of a similar inviscid rotating hydraulic control theory as a constraint on the flow through several ocean channels shows a similar tendency toward theoretical predictions of transport significantly larger than observed values (Whitehead 1989, his Table 1). Recently, it has been shown that changes in upstream conditions and control section geometry for channels
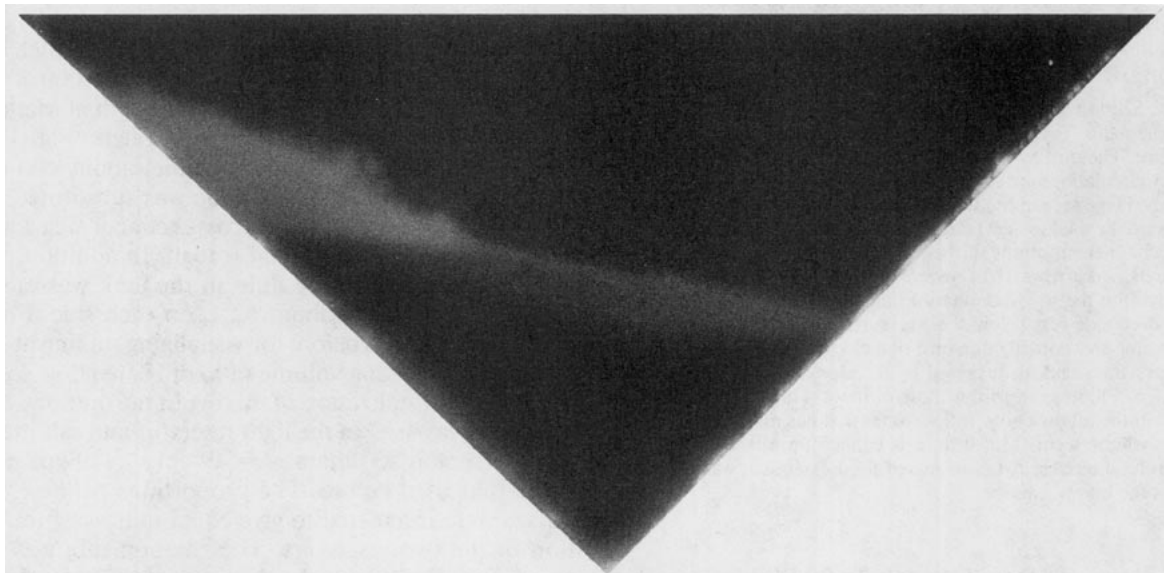

FIG. 6. End view of fluorescein in the turbulent trough experiment (oriented as in Fig. 1b). The light sheet was 45 cm from the inflow entry, near the middle of the channel. The wedge-shaped interface is sharpened at the deep (right) side by the strain field resulting from the solid boundary Ekman flows moving toward it in both layers, and spread at the shallow (left) side by advection of mixed fluid along the interface toward the shallow (left) side by the secondary circulations. This wedge shape is similar to the pycnocline in some ocean straits (cf. Johnson and Sanford 1992; their Fig. 6).

much wider than the Rossby radius can greatly reduce these overestimates without resorting to friction (Killworth 1992). Our experiments have shown that a balance among acceleration, friction, and changes in interface height can also reduce the transport through a rotating channel of a width similar to the Rossby radius by inducing an alongchannel interface slope. Secondary circulations further limit frictionally modified rotating hydraulic exchange by efficiently spinning down the interior flow. Theories for frictionally modified rotating hydraulic exchange should be developed that include the effects of the secondary circulation and possibly the alongchannel variations in interface height within the context of rotating hydraulic control. A numerical model that includes friction and rotation gives transport predictions for a square channel that are closer to the observed values than those reported here (Hallberg and Rhines 1992, personal communication). While this model is two-dimensional, just including the cross-channel circulation improves transport predictions considerably.

Pictures of the experiments reveal a set of secondary circulations driven by interfacial and solid-boundary Ekman layers. Water parcels execute helical motions as they flow through the channel. Evidence for robust interfacial Ekman layers is shown. In the trough, the dominant secondary circulations in each layer are clockwise looking downstream. Dense water in the outflow is advected toward the deep side of the trough along the bottom. Light water in the inflow is also advected toward the deep side on this wall. In the inflow, mixed fluid is swept across the interface toward the shallow side. In the outflow, the interfacial secondary circulation exists only on the shallow side. In the trough, a wedge-shaped interface is generated, especially for high Reynolds number flows. The strain field generated by the cross-channel secondary circulations sharpens the deep side of the interface, which spreads toward the shallow side owing to mixing and the strain field.

Limited velocity data in the center of the Faroe Bank Channel suggest a cross-channel Ekman flow at the bottom with a return circulation in the pycnocline (Johnson and Sanford 1992). This pattern is simpler than that observed in the laboratory, at least for laminar flow in a trough. If the stress at the Faroe Bank Channel walls is increased by the rough surfaces there, the solid-boundary secondary circulations may overwhelm the interfacial secondary circulations, resulting in the observed pattern. In addition, turbulent mixing and continuous stratification may alter the Ekman dynamics within the pycnocline.

REFERENCES

Armi, L., and D. M. Farmer, 1989: The flow of Mediterranean water through the Strait of Gibraltar. *Progress in Oceanography*, Vol. 21, Pergamon 1–105.

Batchelor, G. K., 1967: *An Introduction to Fluid Dynamics.* Cambridge University Press, 615 pp.

Benton, G. S., and D. Boyer, 1966: Flow through a rapidly rotating conduit of arbitrary cross-section. *J. Fluid Mech.*, **26**, 69–79.

Borenäs, K., and P. Lundberg, 1986: Rotating hydraulics of flow in a parabolic channel. *J. Fluid Mech.*, **167**, 309–326.

——, and ——, 1988: On the deep-water flow through the Faroe Bank Channel. *J. Geophys. Res.*, **93**, 1281–1292.

Breidenthal, R., 1981: Structure in turbulent mixing layers and wakes using a chemical reaction. *J. Fluid Mech.*, **109**, 1–24.

Bryden, H. L., and T. H. Kinder, 1991: Steady two-layer exchange through the Strait of Gibraltar. *Deep-Sea Res.*, **38** (Suppl. 1), S445–S463.

Crease, J., 1965: The flow of Norwegian Sea Water through the Faroe Bank Channel. *Deep-Sea Res.*, **12**, 143–150.

Dalziel, S. B., 1990: Rotating two-layer sill flows. *The Physical Oceanography of Sea Straits*, L. J. Pratt, Ed., Kluwer Academic 343–371.

Gidhagen, L., and B. Håkansson, 1992: A model of deep water flow into the Baltic Sea. *Tellus*, **44**, 414–424.

Gill, A. E., 1977: The hydraulics of rotating-channel flow. *J. Fluid Mech.*, **80**, 641–671.

Hart, J. E., 1971: Instability and secondary motion in a rotating channel flow. *J. Fluid Mech.*, **45**, 341–351.

Helfrich, K. R., 1991: Unsteady two-layer exchange flows through a contraction. *Eos, Trans. Am. Geophys. Union*, **72**(51) (Suppl.), 33.

Hogg, N. G., 1983: Hydraulic control and flow separation in a multilayered fluid with applications to the Vema Channel. *J. Phys. Oceanogr.*, **13**, 695–708.

Johnson, G. C., and T. B. Sanford, 1992: Secondary circulation in the Faroe Bank Channel outflow. *J. Phys. Oceanogr.*, **22**, 927–933.

Johnson, D. A., S. E. McDowell, L. G. Sullivan, and P. E. Biscaye, 1976: Abyssal hydrography, nephelometry, currents, and benthic boundary layer structure in the Vema Channel. *J. Geophys. Res.*, **81**, 5771–5786.

Killworth, P. D., 1992: Flow properties in rotating, stratified hydraulics. *J. Phys. Oceanogr.*, **22**, 997–1017.

Koochesfahani, M. M., and P. E. Dimotakis, 1986: Mixing and chemical reactions in a turbulent liquid mixing layer. *J. Fluid Mech.*, **170**, 83–112.

Lundberg, P., 1983: On the mechanics of deep-water flow in the Bornholm Channel. *Tellus*, **35**, 149–158.

Ochoa, J., and N. A. Bray, 1991: Water mass exchange in the Gulf of Cadiz. *Deep-Sea Res.*, **38**(Suppl. 1), S465–S503.

Pedlosky, J., 1979: *Geophysical Fluid Dynamics.* Springer-Verlag, 624 pp.

Prandtl, L., and O. G. Tietjens, 1934: *Applied Hydro- and Aerome-chanics,* McGraw-Hill, 311 pp.

Pratt, L. J., 1986: Hydraulic control of sill flow with bottom friction. *J. Phys. Oceanogr.,* **16,** 1970–1980.

——, and P. A. Lundberg, 1991: Hydraulics of rotating strait and sill flow. *Annu. Rev. Fluid Mech.,* **23,** 81–106.

Reid, J. L., 1979: On the contribution of the Mediterranean Sea outflow to the Norwegian–Greenland Sea. *Deep-Sea Res.,* **26,** 1199–1223.

Rydberg, L., 1980: Rotating hydraulics in deep-water channel flow. *Tellus,* **32,** 77–89.

Saunders, P. M., 1990: Cold outflow from the Faroe Bank Channel. *J. Phys. Oceanogr.,* **20,** 29–43.

Whitehead, J. A., 1989: Internal hydraulic control in rotating fluids—Applications to oceans. *Geophys. Astrophys. Fluid Dyn.,* **48,** 169–192.

——, A. Leetmaa, and R. A. Knox, 1974: Rotating hydraulics of strait and sill flow. *Geophys. Fluid Dyn.,* **6,** 101–125.